Fluid structure interaction of Francis-99 turbine and experimental validation

IOP Conf. Series: Journal of Physics: Conf. Series **1296** (2019) 012006 doi:10.1088/1742-6596/1296/1/012006

Fluid structure interaction of Francis-99 turbine and experimental validation

Petter T. K. Østby[1,3], Einar Agnalt[2], Bjørn Haugen[3], Jan Tore Billdal[1], Ole Gunnar Dahlhaug[2]

1:Rainpower AS, 2027 Kjeller, Norway
2:Waterpower Laboratory, Department of Energy and Process Engineering, NTNUNorwegian University of Science and Technology, Trondheim, Norway
3:Waterpower Laboratory, Department of Mechanical and Industrial Engineering, NTNUNorwegian University of Science and Technology, Trondheim, Norway

E-mail: petter.oestby@rainpower.no

Abstract. The ability to predict a francis runners dynamic response to the exciting forces is paramount to avoid unwanted disintegration of the turbines components. In this article, each of the principal factors contributing to the dynamic response of the runner; eigenfrequency, mode shape, damping and pressure force, is individually examined and compared to the measured values from the Francis-99 runner. Even though the runner is made with a bolted connection between the blades and crown/band, and thus severely increasing the complexity, quite accurate predictions are possible using methods previously validated for massive and symmetric runners. All calculations are conducted on the best efficiency point and with eigenmodes corresponding to Nodal Diameter 4 as excited by the second harmonic of the guide vane passing frequency. The calculated natural frequency for the first two ND4 eigenmodes are within ±5% of the measured values. Further are the calculated eigenmodes, forcing pressure field and hydrodynamic damping all within measurement tolerances with some minor exceptions.

1. Introduction

The ability to calculate the Fluid Structure Interaction on a submerged structure in flowing water is the theme of the third iteration of the Francis-99 workshops. Lots of research have previously been conducted on the different aspects of FSI on Francis runners as summarized by Trivedi and Soltani [1, 2, 3]. The Francis-99 runner proposes a unique challenge as it is made out of blades mounted on flanges which are bolted to the crown and band. Further, the trailing edge of the full blade is not fixed to the band allowing for very large vibration amplitudes in this region compared to a conventional runner blade. The runner also gives a unique opportunity to verify the numerical codes as two eigen frequencies of the runner coincide with the second harmonic of the guide vane passing frequency revealing data for the damping, eigen frequencies, eigenmodes and pressure field as shown by Agnalt et al. [4]. In this article we conduct the necessary

numerical calculation for each of the above mentioned phenomena and compare the results with the measured values.

2. Theory

The linear response of a structure submerged in compressible water exposed to an external force $\mathbf{F}$ can be described through equation 1 [5].

$$\begin{bmatrix} \mathbf{M} & \mathbf{0} \\ -\rho\mathbf{L}^T & \mathbf{Q} \end{bmatrix} \begin{Bmatrix} \ddot{\mathbf{u}} \\ \ddot{\mathbf{p}} \end{Bmatrix} + \begin{bmatrix} \mathbf{B} & \mathbf{0} \\ \mathbf{0} & \mathbf{C} \end{bmatrix} \begin{Bmatrix} \dot{\mathbf{u}} \\ \dot{\mathbf{p}} \end{Bmatrix} + \begin{bmatrix} \mathbf{K} & \mathbf{L} \\ \mathbf{0} & \mathbf{H} \end{bmatrix} \begin{Bmatrix} \mathbf{u} \\ \mathbf{p} \end{Bmatrix} = \begin{Bmatrix} \mathbf{F} \\ \mathbf{0} \end{Bmatrix} \tag{1}$$

Here $\mathbf{M}, \mathbf{B}, \mathbf{K}$ describes the mechanical system properties $\mathbf{Q}, \mathbf{C}, \mathbf{H}$ describes the compressible fluid and $\mathbf{L}$ is the coupling matrix between the fluid and structure. $\mathbf{u}$ and $\mathbf{p}$ are the displacements and pressures.

The equation does not take into account effects of fluid flow nor gyroscopic effect due to rotation. Both terms are assumed negligible. The pressure p is modeled as a acoustic pressure in the fluid distinct and not interacting with the external convective pressure constituting the external force F.

To simplify the solution of the above equation the system can be rearranged into a set of undamped orthogonal eigenmodes, $\mathbf{\Phi}_i$ with corresponding eigenvalues $\lambda_i = \omega_i^2$. Further assuming that the damping can be described as an individual damping ζ_i for each mode without cross coupling, we get equation (2) for each eigenmode i with motion q_i.

$$\ddot{q}_i + 2\zeta_i\omega_i\dot{q}_i + q_i\omega_i^2 = \mathbf{\Phi}_i^T\mathbf{F}(t) \tag{2}$$

As long as the problem is linear and orthogonal we can thus estimate the dynamic response of the structure by computing each individual property: ω_i , ζ_i , $\mathbf{\Phi}_i$ and $\mathbf{F}(t)$.

2.1. Hydrodynamic damping

As shown by several authors [6, 7, 8], the damping created by the flow along a vibrating blade can be significant, dominating over any structural damping. Both theory and experiments conclude that the damping will likely increase linearly with the water velocity. This holds true at least for velocities where the shedding frequency is above the eigenfrequency.

In short, we can calculate the hydrodynamic damping by using the fact that only damping will contribute any net work integrated over one vibration period.

$$\begin{aligned} q_i(t) &= q_i \cdot sin(\omega t) \\ \oint 2\zeta_i\omega_i q_i cos(\omega t)dx &= \oint \mathbf{\Phi}_i^T\mathbf{F}(t)dx \end{aligned} \tag{3}$$

Completing the integral on the left side of equation (3) and noticing that the right side is the external work done by the structure on the fluid W_f due to the vibration of the relevant eigenmode, we can rearrange the equation (3) to equation (4).

$$\zeta_i = \frac{W_f}{2\pi\omega_i^2 q_i^2} \tag{4}$$

In equation above the denominator includes values which can be found in a modal analysis. The external work can be found using CFD software with mesh motion according to the relevant eigenmode.

3. Test case

The geometries used in this article are based on those provided with the Francis-99 [9] workshop. It is a low specific speed runner with 15 full blades and 15 splitter blades, 28 guide vanes and an outlet diameter of $D_2 = 349\,mm$. The runner is mounted with four pressure sensors in one channel (R1,R2,R3,R4) as shown in Figure 1. The runner is made out of a massive crown and a massive band. Each blade is placed on a flange that fits into a slot on the crown and band. Each blade is fixated with four bolts through the crown and band. The last 90 *mm* of the full blade at the band towards the trailing edge is not connected to neither the flange nor the band leaving it hanging freely.

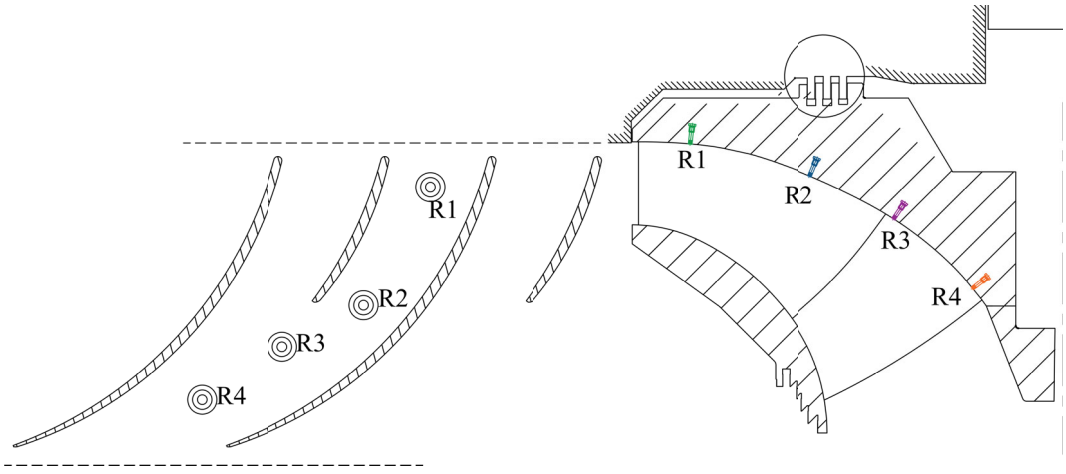

Figure 1: Location of pressure sensors in the Francis 99 runner[9]

By varying the speed of the unit, while keeping the unit speed and unit discharge at BEP values, Agnalt et. al. [4] were able to detect a resonance in the runner. As the resonance is excited by the second harmonic of the guide vane passing frequency the resulting Nodal Diameter will be $2 \cdot (15 + 15) - 2 \cdot 28 = 4$. The operating points used are shown in Table 1.

By decomposing the measurements into acoustic and convective pressure models, two eigen frequencies with their corresponding damping and eigenmodes were identified. Hereafter named mode A and mode B. Some of the key results are shown in Table 2.

4. Numerical models

4.1. Geometrical preparation

A few simplifications of the geometry was made to ease the numerical calculations.

Description	Flow Rate $[m^3/s]$	nED	QED	Head $[m]$	Speed $[rpm]$
BEP-1	0.134	0.179	0.154	5.2	219.8
BEP-2	0.160	0.176	0.156	7.2	254.3
BEP-3	0.183	0.178	0.154	9.6	297.8
BEP-4	0.209	0.178	0.155	12.6	340.5
BEP-5	0.232	0.180	0.154	15.55	381.7

Table 1: Operating points used to identify resonance parameters on the Francis 99 model

Mode	eigenfrequency $[Hz]$	Damping [%]
A	272.5 ± 0.9	$n \cdot (0.013361 \pm 0.0013)$
B	325.5 ± 2.7	$n \cdot (0.021299 \pm 0.0033)$

Table 2: Calculated eigenfrequencies and equation for damping (n is speed in rpm) for ND4 in the Francis 99 runner [4]

- All fillets between blades and crown/band has been removed
- The free trailing edge has been lifted $0.2mm$ off the band ensuring no contact. It is however assumed that no water runs beneath the blade
- All holes, both for bolts and measurement equipment has been removed

4.2. Modal Analysis

As the simplified runner geometry is rotational periodic, only $1/15th$ of the runner is used in the calculation and a symmetric boundary condition is used on the periodic boundaries. An acoustic domain is used to model the water inside of the runner and between the runner and covers. The covers are assumed rigid. To simplify the meshing, the domain was increased around the sealing surfaces. Normally this could affect the eigenfrequency as the tight space between the runner and seals could significantly increase the added mass, however as the blade is not fixated at the trailing edge towards the band, we can expect less deformation in this region and thus less effect of the tight seals.

The water domain is limited at $R = 345mm$ and $Z = 191mm$ and the boundaries are modelled as hard walls. A fixed support is added to the runner flange. The blades are assumed to only connect to the crown and band at the location of the bolts. All material properties used in the calculation is shown in Table 3. The calculation is done in Ansys v19.2.

The eigen frequencies and acoustic pressures have been extracted at the location of the pressure sensors in the runner.

	Material	Young's Modulus $[GPa]$	Density $[kg/m^3]$	Poisson's ratio $[-]$	Speed of Sound $[m/s]$
Crown Band	JM7	110	7600	0.32	-
Blades	JM3	100	8800	0.3	-
Water	Water	-	1000	-	1483

Table 3: Material properties used in modal analysis

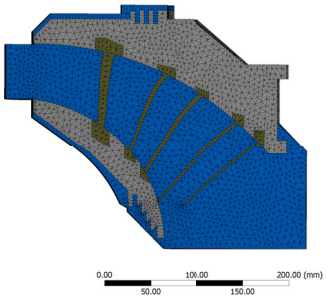

Figure 2: Numerical Domain with 3.3 mm mesh

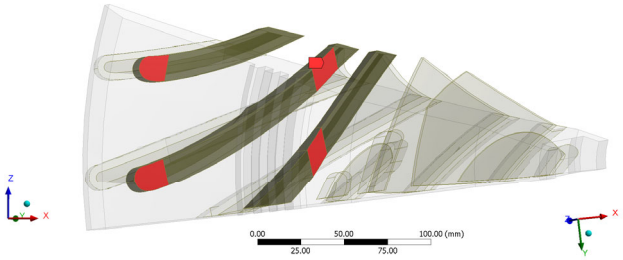

Figure 3: Bonded connection location between blades and band

4.3. Pressure loading

To calculate the dynamic pressure loading on the runner from the guide vanes, a transient CFD calculation was set up using Ansys CFX v19.2. The method is typical to determine the pressure loading from RSI and has been tested and verified several times before [10, 11]. Only the runner and guide vanes are included. As there are no symmetry lines with 28 guide vanes and 15 runner full blades, the whole 360 has to be included. A fixed mass flow is given at the inlet and a rotational speed according to BEP-4 in Table 1 and a constant pressure opening is used at the outlet.

The calculation is run with 1400 time steps per rotation and the pressure signal at the location of the pressure sensors are extracted once they have settled into a steady periodic signal.

The mesh is purely structured with only prism elements. A k-epsilon turbulence model was used with a y+ in the range of 20-50.

4.4. Hydrodynamic damping

To calculate the damping induced by the flowing water a setup with three runner blade passages simulated in Ansys CFX v19.2. The inlet boundary condition is taken from a stationary CFD calculation with runner and guide vanes. At the outlet, a constant pressure opening is used. A rotational periodic boundary condition is used. The complex mode shape as calculated in the modal analysis was imposed as mesh motion on the three full and splitter blades with a given amplitude. The mesh was similar to that used to calculate the pressure loading as described above with a y+ in the range of 20-50

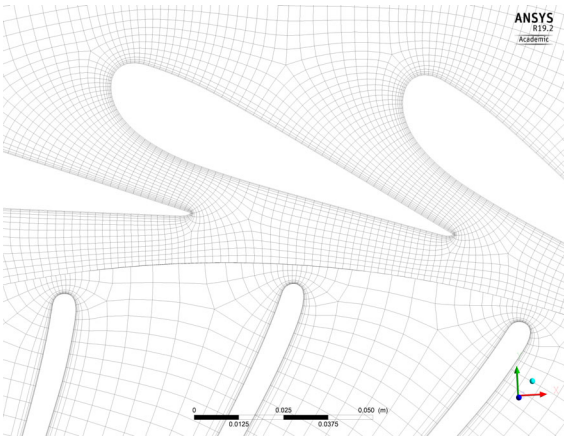

Figure 4: Section of the mesh used to calculate the pressure loading on the blades

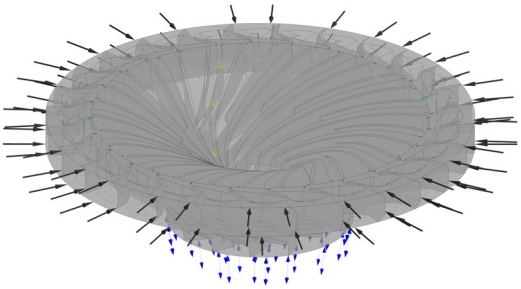

Figure 5: Calculation domain for the transient CFD

and about 250k mesh elements for each runner channel. Extra care was taken to ensure good resolution of the mesh in the regions with the greatest mesh deformation. The k-epsilon turbulence model was used.

Even though three blades are not enough to have a valid symmetry condition on the periodic edges with a ND4 motion of the blades, by only investigating the middle blade and assuming that the neighbour blades shield the center blade from the error in the periodic condition we can use this setup. The validity of this approach has been verified by Nenneman et al. [12].

One case was run for each of the operating points shown in Table 1. The work done by the steel structure to the water integrated over one period, as calculated by equation 5, was extracted after five oscillation periods. Then the value has usually settled.

$$W_f = \oint \int_A p\vec{v} \cdot \hat{n} \, dA \, dt \tag{5}$$

5. Results

5.1. Eigenfrequency

The calculated eigenfrequency for the first two ND4 modes are $260Hz$ and $337Hz$. Compared to the measured values $272.5Hz$ and $325.5Hz$ these values are within $\pm 5\%$. A mesh independence study was conducted which reveals that Mode A is not particularly dependant on mesh size, while Mode B changes more with mesh size, see Figure 7. With a mesh size of $5mm$ the values have converged well. The frequency of Mode A is somewhat under predicted. Normally the FE model is to stiff, over predicting the frequency. In the numerical model the fillets are removed reducing the runners overall stiffness.

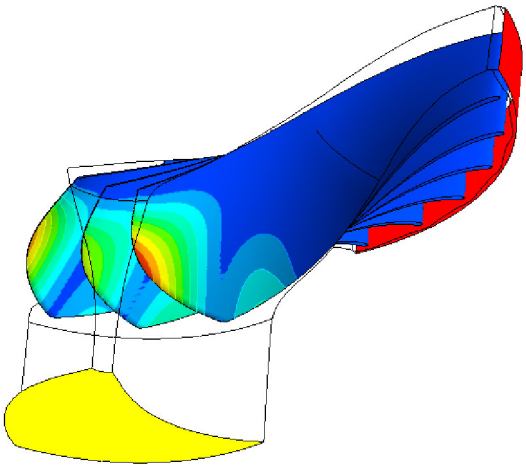

Figure 6: Domain used used to calculate the hydrodynamic damping. Inlet in red and outlet in yellow. Blades shown with real component of mesh deformation for mode B.

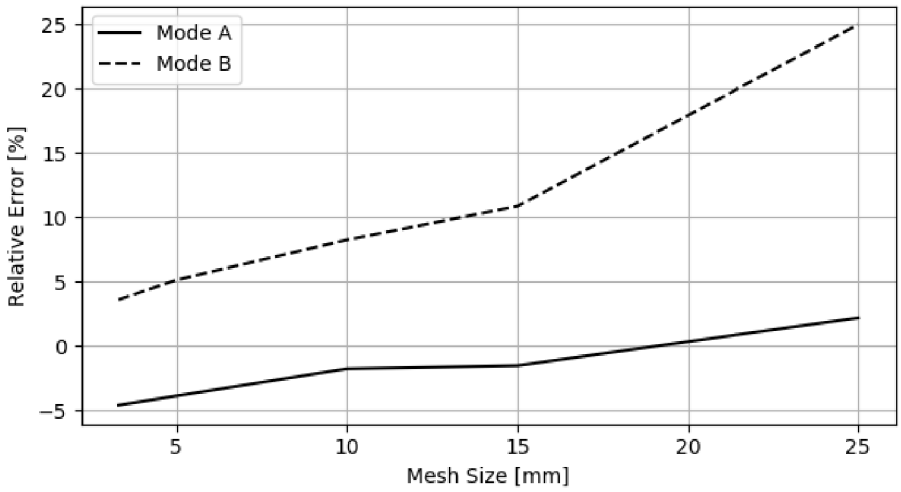

Figure 7: Mesh independence study for the two first eigenmodes of ND4.

5.2. Mode shape

Both the calculated eigenmodes have the majority of their deformation on the trailing edge of the blade. While mode A have the largest vibrations towards the band and the free edge mode B have larger vibrations towards the crown as shown in Figure 8.

The calculated acoustic pressure for each mode at the location of the pressure sensors have been extracted and compared to the values found by Agnalt [4]. As the mode shape is complex and only of relative scale, the numerical results have been rotated and scaled to best fit with the experimental data.

A comparison between the measured and numerical eigenmodes are shown in Figure

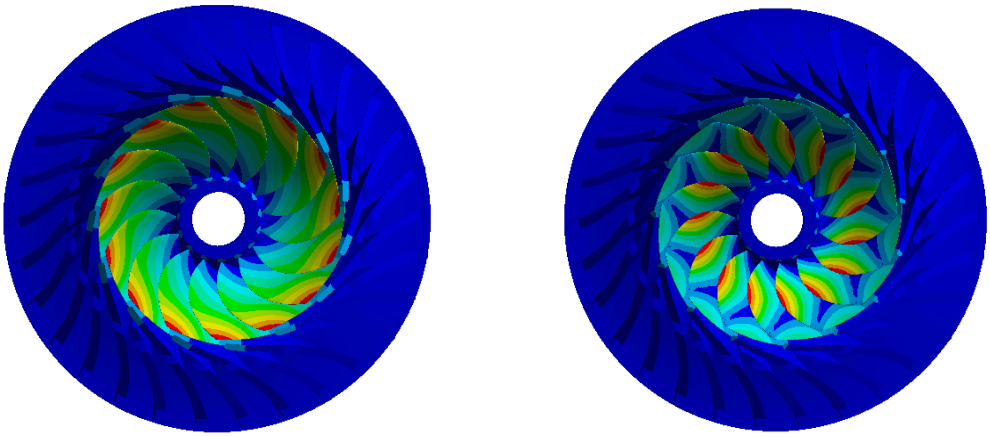

Figure 8: Vibration Amplitudes for the two eigenmodes, A and B. Both modes are ND4, but displayed here as ND0 to emphasize the difference in mode shape amplitudes. Here shown without runner band

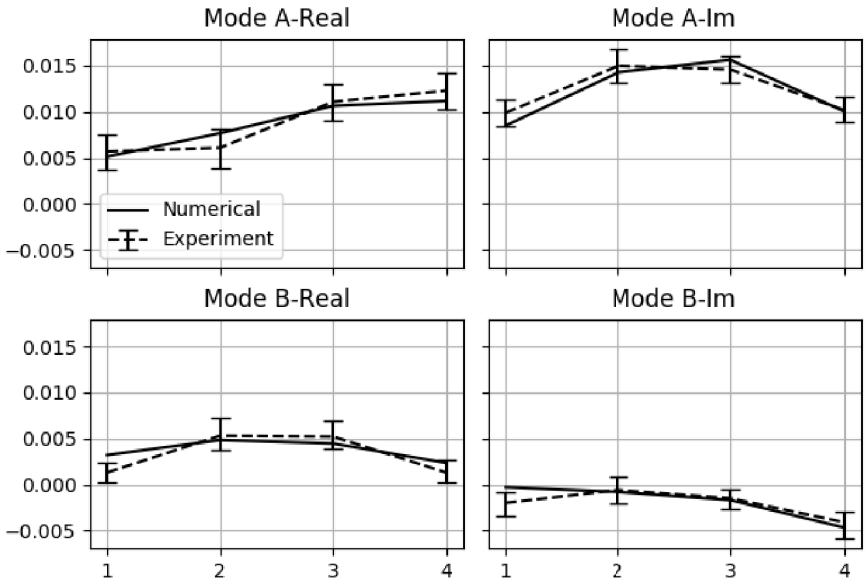

Figure 9: Comparison of the complex pressure eigenmodes, Measured and Numerical values for sensors R1-R4 using 3.3 *mm* mesh size.

9. For mode A, all the calculated values are within the measurement uncertainty. For mode B, the values calculated at sensor R1 are outside of the measurement uncertainty. This may be due to the simplification at the runner inlet where a fixed wall is placed, while the real turbine has a time varying boundary condition as seen by the runner as it rotates behind the guide vanes. This time varying condition is a non-linearity that cannot be included in the type of analysis conducted here.

5.2.1. Pressure loading By monitoring the pressure signal and extracting the second harmonic of the guide vane passing frequency using a FFT algorithm, we can compare the numerical results to the measured values. The results are shown in Figure 10. The pressure amplitudes are captured quite well with the CFD, however the CFD has a larger phase variation between the sensors than what is found in the measurements.

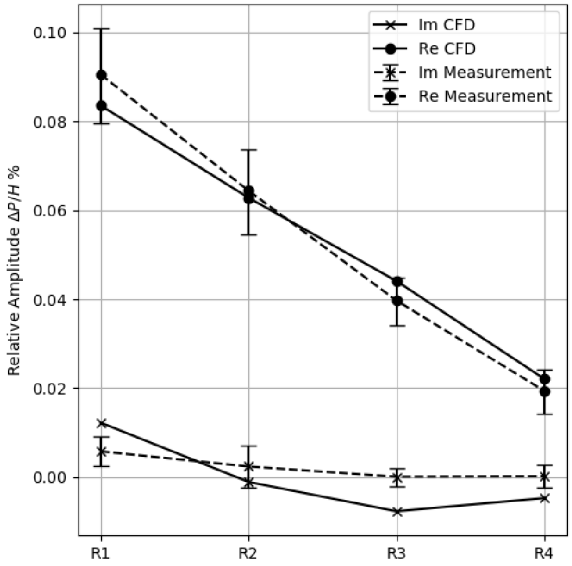

Figure 10: Comparison of the convective pressure field in the runner between CFD and measurements for the second harmonic of the guide vane passing frequency.

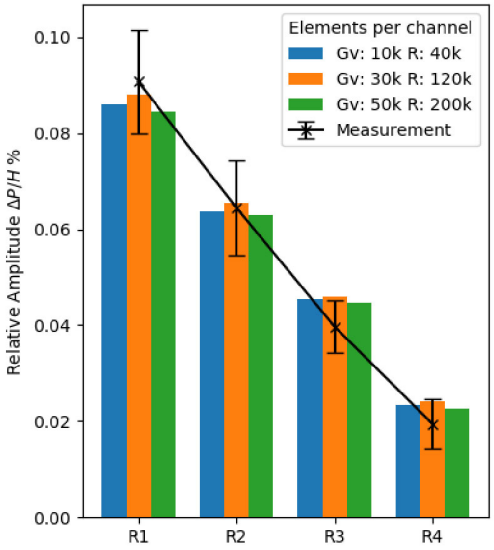

Figure 11: Pressure amplitudes calculated in the runner with different number of elements per guide vane (GV) and runner (R) channels.

The results are not very mesh dependent. Going from 10k elements per guide vanes channel and 40k elements per runner channel to 50k elements per guide vanes channel and 200k elements per runner channel hardly changes calculated values.

5.3. Hydrodynamic damping

The damping was calculated for both modes at all operating points. A vibration amplitude of 0.01mm was used. For mode B the sensitivity of time steps per oscillation period was investigated. The results are shown in Figure 12. With 256 time steps per period for Mode B the results converge to the measured values for all speeds.

Mode A is only calculated with 256 time-steps. The average value of Mode A is quite close to the measure value while the slope of the curve is higher in the numerical calculations. The exact reason is unknown, however mode A has the largest vibrations in the region of the loose blade edge which is simplified in the numerical model creating larger modeling uncertainties for mode A than mode B. Trailing part of the blade may have some small area where it makes contact with the band thus changing the hydrodynamic damping. Another possibility is that with increased speed and head,

the gap actually increases allowing for a through flow of water between the blade and the band. This may puncture the local pressure difference across the bland and thus reducing the hydrodynamic damping. This effect is not captured in the CFD as no flow is allowed to pass in the gap between blade and band.

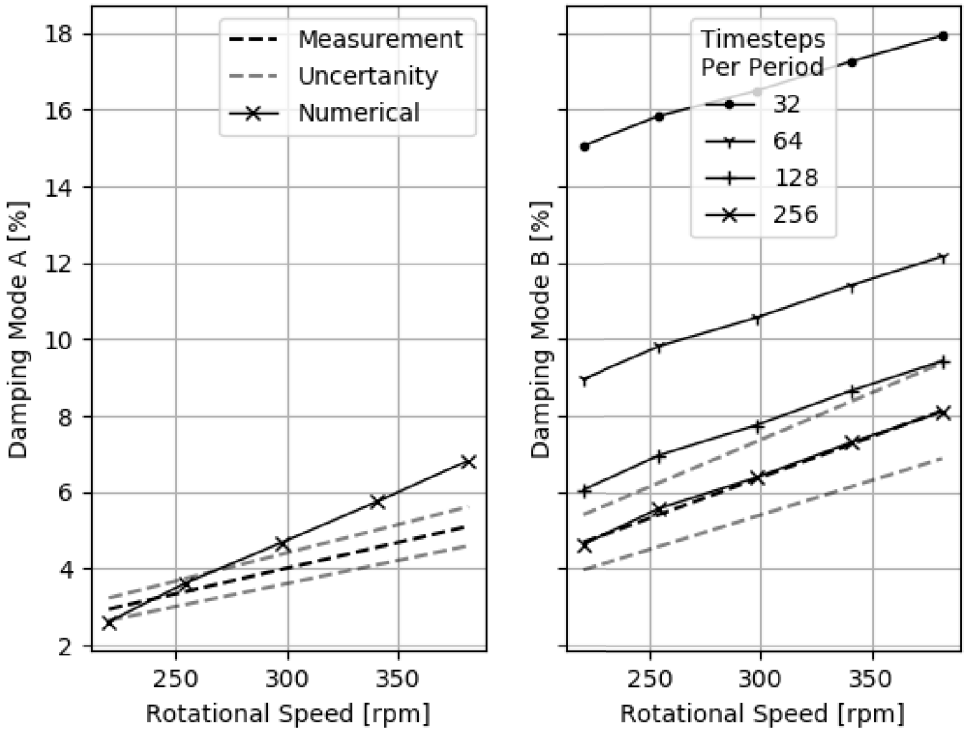

Figure 12: Calculated hydrodynamic damping for the two modes as a function of rotational speed.

6. Conclusion

Calculating the dynamic response of the Francis-99 runner is particularly difficult as it is made out of blades mounted on flanges which are bolted to the crown and band. Further is the trailing edge of the full blade not fixed to the band.

Using already developed methods which have been verified on massive runners we have shown that they, also in the case of the Francis-99 runner, are able to calculate the measured values to within engineering required precision:

- Eigen frequencies within ±5% of measured values
- Acoustic eigenmodes are within measurement tolerances for all points except one
- Convective pressure amplitudes are within measurement tolerances with some deviations to the phase angle.

- The calculated hydrodynamic damping is well within the measured uncertainty bands for mode B, but the slope of the damping curve does not fit well for mode A. This may be due to varying degree of contact between the blade and band.

References

[1] Chirag Trivedi. A review on fluid structure interaction in hydraulic turbines: A focus on hydrodynamic damping. *Engineering Failure Analysis*, 77(Supplement C):1 – 22, 2017.

[2] Chirag Trivedi and Michel J. Cervantes. Fluid-structure interactions in francis turbines: A perspective review. *Renewable and Sustainable Energy Reviews*, 68(Part 1):87 – 101, 2017.

[3] Arash Soltani Dehkharqani, Jan-Olov Aidanp, Fredrik Engstrm, and Michel Cervantes. A review of available methods for the assessment of fluid added mass, damping, and stiffness with an emphasis on hydraulic turbines. *Applied Mechanics Reviews*, 70:20, 12 2018.

[4] Einar Agnalt, Petter Ostby, Bjorn W. Solemslie, and Ole G. Dahlhaug. Experimental study of a low-specific speed francis model runner during resonance. *Shock and Vibration*, Article ID 5796875:12, 2018.

[5] G.C. Everstine. Finite element formulations of structural acoustic problems. *Computers & Structures*, 65:307–321, 11 1997.

[6] C Monette, B Nennemann, C Seeley, A Coutu, and H Marmont. Hydro-dynamic damping theory in flowing water. *IOP Conference Series: Earth and Environmental Science*, 22(3):032044, mar 2014.

[7] A Coutu, C Seeley, C Monette, B Nennemann, and H Marmont. Damping measurements in flowing water. *IOP Conference Series: Earth and Environmental Science*, 15(6):062060, 2012.

[8] Carl W. Bergan, Bjørn W. Solemslie, Petter Østby, and Ole G. Dahlhaug. Hydrodynamic damping of a fluttering hydrofoil in high-speed flows. *International Journal of Fluid Machinery and Systems*, 11(2):146–153, 2018.

[9] Chirag Trivedi and Ole G. Dahlhaug. Francis 99 : A test-case a test-case on a high head francis turbine. 2019.

[10] Ken-Robert G. Jakobsen, Erik Tengs, and Martin Aa. Holst. Reducing computational effort of high head francis turbines. *IOP Conference Series: Earth and Environmental Science*, 240:072001, mar 2019.

[11] B. Nennemann, T.C. Vu, and M. Farhat. Cfd prediction of unsteady wicket gate-runner interaction in francis turbines: A new standard hydraulic design procedure. *HYDRO 2005*, 2005.

[12] Bernd Nennemann, Christine Monette, and Jol Chamberland-Lauzon. Hydrodynamic damping and stiffness prediction in francis turbine runners using CFD. *IOP Conference Series: Earth and Environmental Science*, 49:072006, nov 2016.